Effective in-device r_{33} of 735 pm/V on electro-optic polymer infiltrated silicon photonic crystal slot waveguides

Xiaolong Wang,[1,*,†] Che-Yun Lin,[2,†] Swapnajit Chakravarty,[1] Jingdong Luo,[3] Alex K.-Y. Jen,[3] and Ray T. Chen[2]

[1]*Omega Optics, Inc., 10435 Burnet Road, Suite 108, Austin, Texas 78758, USA*

[2]*Department of Electrical and Computer Engineering, University of Texas at Austin, Austin, Texas 78758, USA*

[3]*Department of Materials Science and Engineering, University of Washington, Seattle, Washington 98195, USA*

**Corresponding author: alan.wang@omegaoptics.com*

Received November 5, 2010; accepted January 12, 2011;
posted January 26, 2011 (Doc. ID 137690); published March 9, 2011

We design and fabricate a 320 nm slot for an electro-optic (E-O) polymer infiltrated silicon photonic crystal waveguide. Because of the large slot width, the poling efficiency of the infiltrated E-O polymer (AJCKL1/amorphous polycarbonate) is significantly improved. When coupled with the slow light effect from the silicon photonic crystal waveguide, an effective in-device r_{33} of 735 pm/V, which to our knowledge is a record high, is demonstrated, which is ten times higher than the E-O coefficient achieved in thin film material. Because of this ultrahigh E-O efficiency, the $V_\pi L$ of the device is only 0.44 V mm, which is to our knowledge the best result of all E-O polymer modulators.

OCIS codes: 230.4110, 230.5298.

Electro-optic (E-O) polymer modulators have demonstrated exceptional performance for ultrahigh bandwidth [1] and subvolt half-wave driving voltage (V_π) [2–4]. However, the improvement of E-O polymer photonic devices is limited by conventional waveguide structures with micrometer-sized features. The flourishing of silicon nanophotonics, especially silicon slot waveguides [5] and photonic crystal waveguides [6–8], provides a platform for E-O polymer integration into nanometer scale waveguides; for instance, E-O polymer infiltrated slot waveguides [9–12]. Nevertheless, the in-slot E-O efficiency is relatively low (~10% – 30%) compared with the r_{33} value provided by the E-O polymer. The mechanism that hinders the E-O poling efficiency in narrow slot waveguides is not yet fully understood. Recent research has shown that large leakage current during the poling process can degrade the poling efficiency [13]. Using TiO_2 modified electrodes [13] or new E-O polymer materials (such as 15 wt. % AJLZ53/polymethylmethacrylate) [14] with lower conductivity will significantly reduce the leakage current, and it can increase the thin film poling efficiency by more than 40%. Recently, we demonstrated an E-O polymer infiltrated silicon photonic crystal slot waveguide modulator with $V_\pi L$, of 0.56 V mm, and an effective in-device r_{33} of 132 pm/V in the 75 nm slot waveguide [12]. These improvements are attributed to the advanced design using a silicon photonic crystal waveguide, which exploits the slow light effect from the defect mode [15]. However, a relatively low modulation response in the normal light region without slow light enhancement indicates poor E-O poling efficiency. Additionally, the fabrication procedures of 75 nm E-O polymer infiltrated slot waveguides can be challenging both in e-beam lithography and reactive ion etching.

In this Letter, we present physical insight into the increased poling efficiency achieved by wide photonic crystal slot waveguides, and experimentally verify the concept by using a Mach–Zehnder (MZI) structure. The design principle is based on the fact that a wider slot waveguide will significantly suppress the leakage current and thus can increase the poling efficiency. The basic photonic crystal slot waveguide structure is schematically shown in Fig. 1(a). The hexagonal lattice photonic crystal slab waveguide, with a thickness of $t = 230$ nm, has a lattice constant of $a = 425$ nm and a hole diameter of $d = 297$ nm. A W1.3 waveguide (the air hole spacing outside the slot is $W = 1.3\sqrt{3}a$) is chosen, with a total photonic crystal length of 340 μm. The silicon photonic crystal regions including air holes and the slot are fully covered by polymer materials consisting of a guest/host system of 25% weight chromophore AJCKL1 into amorphous polycarbonate (APC). The refractive index of the infiltrated polymer is $n = 163$ at 1.55 μm wavelength. The optical intensity profiles ($|E_x|^2$) of the guided mode at the band edge (wave vector of π/a) is shown in Fig. 1(a) with in-slot optical power around 30%. In this Letter, we investigate the effect of slot width in silicon photonic crystal waveguides. Figure 1(b) shows the simulated band diagrams of photonic crystal slot waveguides with different slot widths in conjunction with two-dimensional cross-sectional views of the optical intensity profiles of the guided modes at the photonic band edges. In Fig. 1(b), the slot mode profile becomes spindlier as the slot width increases, which means that the slot mode inclines to be decoupled into two separate waveguide modes. Additionally, large slot width is detrimental to E-O modulation because the electrodes' separation is increased. Therefore, we believe that a 300 – 350 nm slot width with 30% in-slot power is the optimized design for an E-O polymer infiltrated silicon photonic crystal modulator.

The fabrication procedures for the nanophotonic modulator are described in Ref. [12]. Figure 2(a) shows the scanning electronic microscopy (SEM) image of the silicon photonic crystal slot waveguide. After infiltrating AJCKL1/APC, the sample is heated to the glass transition temperature ($T_g = 145$ °C) of the guest/host polymer while a 86 V/μm poling field is applied. Upon reaching the glass transition temperature, the sample is then cooled

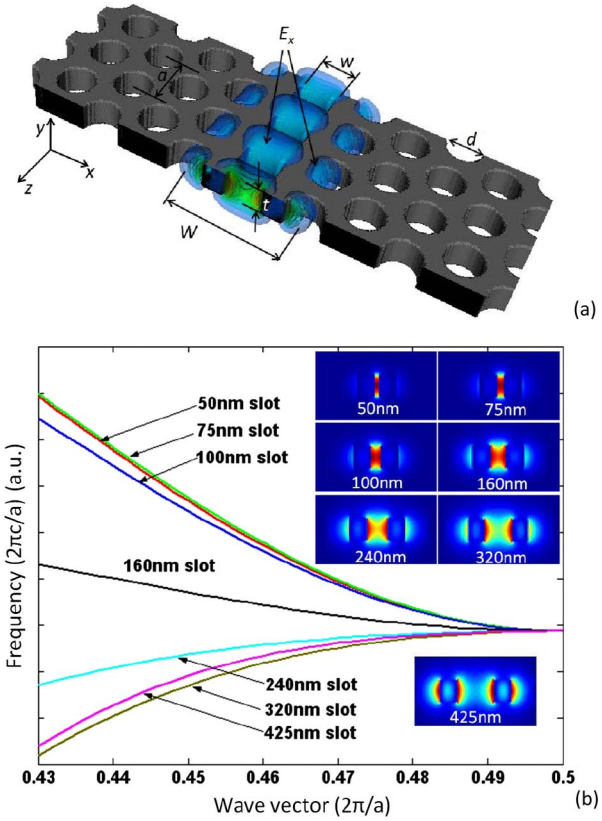

Fig. 1. (Color online) (a) Schematic and simulated optical mode profile of the photonic crystal waveguide with a 320 nm slot, (b) photonic band diagrams and optical mode profiles of different slot widths.

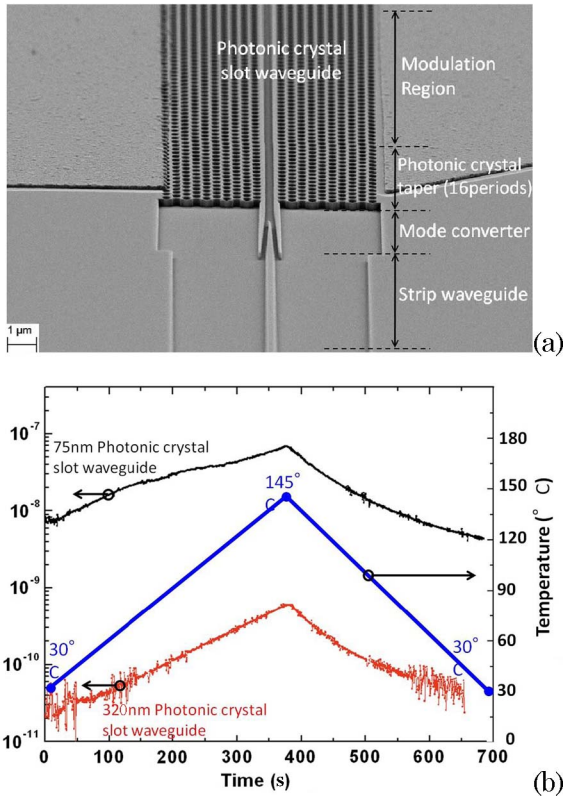

Fig. 2. (Color online) (a) SEM picture of the 320 nm-wide silicon photonic crystal slot waveguide. (b) Leakage current during the poling process for the 75 nm and the 320 nm photonic crystal slot waveguides.

down to room temperature, and the poling voltage is switched off. The leakage current as well as the hot plate temperature during the poling process is monitored *in situ* as shown in Fig. 2(b) for the 75 nm and 320 nm photonic crystal slot waveguides. The peak current for the 75 nm slot is 4.5×10^{-8} A, while it is only 6.2×10^{-10} A for the 320 nm slot. If we assume that the leakage current only goes through the slot waveguide, and a cross-sectional area of $340\,\mu\text{m} \times 0.23\,\mu\text{m}$, the current density of the E-O poling process is $575\,\text{A/m}^2$ and $7.9\,\text{A/m}^2$ for the 75 nm and the 320 nm slots, respectively. Compared with the typical $1 - 10\,\text{A/m}^2$ leakage current of thin film AJCKL1/APC [13], the 320 nm slot waveguide shows comparable leakage current. This significant change of leakage current as a function of the slot width deserves further investigation, in which the device dimension and the silicon/polymer interface are two of the key parameters affecting the materials' conduction mechanism under the poling condition.

In the measurement, the output of the laser source is tuned to a 1539 nm wavelength, where maximum modulation response is achieved. The E-O polymer nanophotonic modulator was driven by a 100 KHz triangular wave with a peak-to-peak voltage, V_{pp}, of 1.7 V. The total optical insertion loss (lensed fiber in, lensed fiber out) is 23 dB, including the 8 dB/facet fiber–waveguide coupling loss. The waveform from a digital oscilloscope in Fig. 3 shows that overmodulation occurs at 1.3 V, which is the V_π of the E-O polymer nanophotonic modulator. The effective in-device E-O coefficient is calculated as

$$\gamma_{33} = \frac{\lambda w}{n^3 V_\pi \Gamma L} = 735\,\text{pm/V}.$$

In this equation, $\Gamma = 0.35$ is the ratio of the optical power that has interactions with the electric field. The r_{33} value of the poled AJCKL1/APC films with 25 wt. % of chromophore loading is 90 pm/V at 1.3 μm, which is measured by the Teng–Man reflection technique. This value corresponds to 70–75 pm/V at 1.55 μm, based on the two-level model approximation [16]. Compared with the thin film r_{33} value, our effective in-device E-O efficiency is

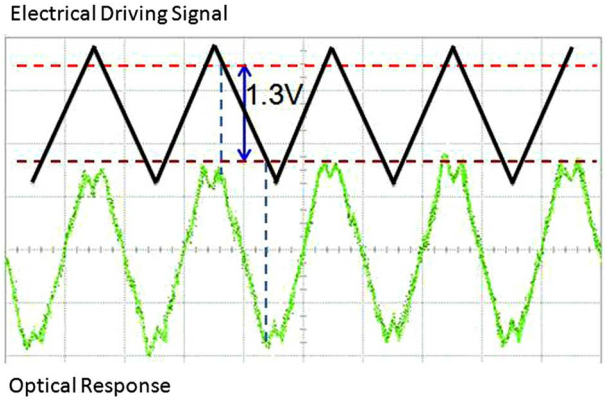

Fig. 3. (Color online) Modulation measurements showing a low V_π of 1.3 V.

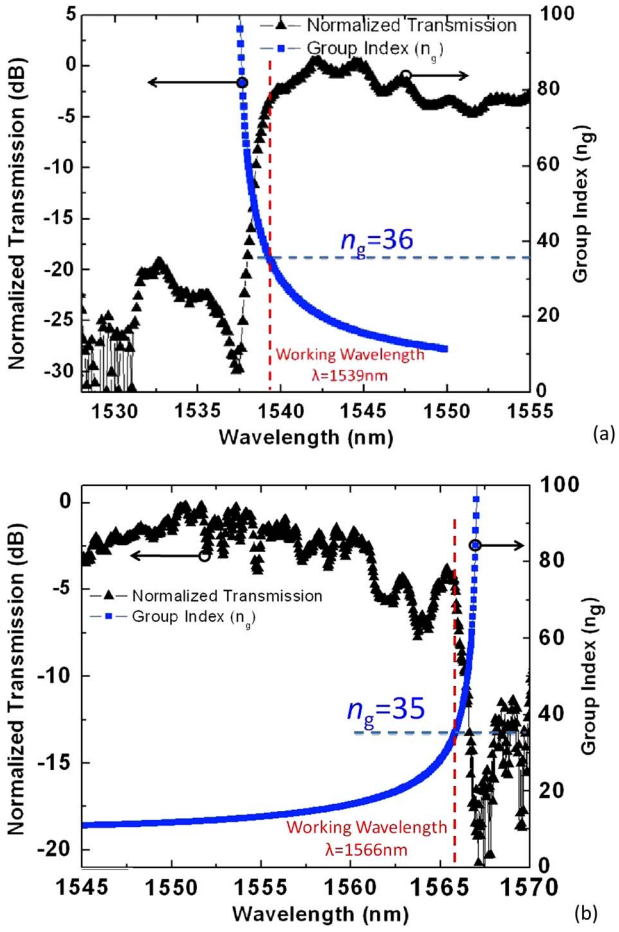

Fig. 4. (Color online) Group indices and optical transmission curves of the E-O polymer infiltrated silicon photonic crystal slot waveguide (a) 320 nm slot and (b) 75 nm slot.

enhanced by almost ten times. This extraordinarily high r_{33} value proves the combined enhancement of slow light effect and an increased poling efficiency.

The nanophotonic modulator also achieves very high modulation efficiency with $V_\pi \cdot L = 1.3\,\mathrm{V} \times 340\,\mu\mathrm{m} = 0.44\,\mathrm{V} \cdot \mathrm{mm}$. This $V_\pi L$ shows 22% improvement over the 0.56 V mm $V_\pi L$ in Ref. [12], which is the best $V_\pi L$ that has ever been reported to our knowledge.

To effectively evaluate the poling efficiency of the E-O polymer inside the photonic crystal slot waveguide, we calculate the group indices of the 320 nm and 75 nm photonic crystal slot waveguides in Figs. 4(a) and 4(b). At the working wavelengths of these two devices, the group indices are 36 and 35 in Figs. 4(a) and 4(b). According to Ref. [17], the slowdown factor, S, of the devices is given as $S = \frac{v_\phi}{v_g} = \frac{n_g}{n_\phi}$, while n_φ is the effective phase index of the waveguide. Considering the field distribution of 30% optical power in E-O polymer and 70% in silicon, n_φ is approximately 2.9. This gives the S of 320 nm and 75 nm photonic crystal slot waveguides as around 12.4 and 12.1, respectively. Given the slow light enhanced effective r_{33}, we can conclude that the material r_{33} from E-O poling is 59 pm/V for the 320 nm slot and 11 pm/V for the 75 nm. The E-O poling efficiency is improved by five times due to the increased slot width.

In summary, we have achieved 735 pm/V effective in-device r_{33} and 0.44 V mm $V_\pi L$, all of which are the best results that have ever been reported, to our knowledge. These improvements are attributed to the increased poling efficiency of the E-O polymer inside the 320 nm photonic crystal slot waveguide. The material r_{33} is calculated to be 59 pm/V by taking account of the slow light enhancement factor. As a comparison, the 75 nm slot only achieves 11 pm/V material r_{33}. By further optimizing the silicon/organic interface and the poling process with more efficient E-O polymer, we expect more significant improvement in device performance of the E-O polymer infiltrated silicon photonic crystal slot waveguide.

The authors would like to acknowledge the Air Force Office of Scientific Research (AFOSR) for supporting this work under the Small Business Technology Transfer Research (STTR) program (grant FA9550-09-C-0086), monitored by Dr. Charles Y.-C. Lee.

†These authors contributed equally to this work.

References

1. D. Chen, H. R. Fetterman, A. Chen, W. H. Steier, L. R. Dalton, W. Wang, and Y. Shi, Appl. Phys. Lett. **70**, 3335 (1997).
2. Y. Shi, C. Zhang, H. Zhang, J. H. Bechtel, L. R. Dalton, B. H. Robinson, and W. H. Steier, Science **288**, 119 (2000).
3. Y. Enami, C. T. Derose, D. Mathine, C. Loychik, C. Greenlee, R. A. Norwood, T. D. Kim, J. Luo, Y. Tian, A. K.-Y. Jen, and N. Peyghambarian, Nat. Photon. **1**, 180 (2007).
4. Y. Enami, D. Mathine, C. T. DeRose, R. A. Norwood, J. Luo, A. K.-Y. Jen, and N. Peyghambarian, Appl. Phys. Lett. **91**, 093505 (2007).
5. V. R. Almeida, Q. Xu, C. A. Barrios, and M. Lipson, Opt. Lett. **29**, 1209 (2004).
6. Y. Jiang, W. Jiang, L. Gu, X. Chen, and R. T. Chen, Appl. Phys. Lett. **87**, 221105 (2005).
7. M. Notomi, E. Kuramochi, and T. Tanable, Nat. Photon. **2**, 741 (2008).
8. D. M. Beggs, T. P. White, L. O'Faolain, and T. F. Krauss, Opt. Lett. **33**, 147 (2008).
9. J. H. Wülbern, J. Hampe, A. Petrov, M. Eich, J. Luo, A. K.-Y. Jen, A. Di Falco, T. F. Krauss, and J. Bruns, Appl. Phys. Lett. **94**, 241107 (2009).
10. T. Baehr-Jones, B. Penkov, J. Huang, P. Sullivan, J. Davies, J. Takayesu, J. Luo, T. D. Kim, L. Dalton, A. Jen, M. Hochberg, and A. Scherer, Appl. Phys. Lett. **92**, 163303 (2008).
11. R. Ding, T. Baehr-Jones, Y. Liu, R. Bojko, J. Witzens, S. Huang, J. Luo, S. Benight, P. Sullivan, J.-M. Fedeli, M. Fournier, L. Dalton, A. Jen, and M. Hochberg, Opt. Express **18**, 15618 (2010).
12. C. Y. Lin, X. Wang, S. Chakravarty, B. S. Lee, W. Lai, J. Luo, A. K.-Y. Jen, and R. T. Chen, Appl. Phys. Lett. **97**, 093304 (2010).
13. S. Huang, T. D. Kim, J. Luo, S. K. Hau, Z. Shi, X. H. Zhou, H. L. Yip, and A. K.-Y. Jen, Appl. Phys. Lett. **96**, 243311 (2010).
14. http://arxiv.org/ftp/arxiv/papers/1009/1009.2336.pdf
15. X. Chen, X. L. Wang, S. Chakravarty, and R. T. Chen, IEEE J. Sel. Top. Quantum Electron. **15**, 1506 (2009).
16. C. Greenlee, A. Guilmo, A. Opadeyi, R. Himmelhuber, R. A. Norwood, M. Fallahi, J. Luo, S. Huang, X.-H. Zhou, A. K.-Y. Jen, and N. Peyghambarian, Appl. Phys. Lett. **97**, 041109 (2010).
17. T. F. Krauss, J. Phys. D **40**, 2666 (2007).